JTTEE5 9:235-240

Enthalpy Measurements of Direct Current Plasma Jets Used for $ZrO_2 \cdot Y_2O_3$ Thermal Barrier Coatings

H.-D. Steffens and T. Duda

(Submitted 15 June 1996; in revised form 15 November 1998)

This study combines enthalpy probe measurements in a direct current (DC) plasma jet under atmospheric conditions and the characterization of sprayed coatings. Two different nozzle diameters were used as anode profiles. A detailed description of the experimental setup is given together with preliminary results. These results emphasize the usability of enthalpy probe measurements in thermal plasma jets for obtaining temperature distributions. For zirconia, the deposition efficiency, density, and structure of the coatings formed with the different anode profiles were compared.

Keywords diagnostics, thermal barrier coatings

1. Introduction

In plasma spraying, plasma composition, enthalpy, temperature, and velocity have a substantial influence on particle acceleration and dwell time, which in turn have a strong effect on particle melting and consequently on the coating structure. The nature of the plasma gas and the power settings, as well as the anode design, determine the plasma jet characteristics. In most cases, when spraying oxides, nozzles are used with an internal diameter of 6 and 8 mm for most commercial plasma torches. With such torches, several problems arise in terms of particle melting due to, for example, the inhomogeneous structure of the plasma jet. These problems can be overcome by using a low velocity plasma torch. Working with an anode with an increased inner diameter, the velocity of the plasma jet is decreased, and the temperature gradients to the fringes are reduced.

Plasma jet characteristics can be evaluated using different techniques. The enthalpy probe technique offers several advantages, such as being relatively inexpensive and simple compared to laser or emission spectroscopy.

In this article, the effect of using anodes with different inner diameters on the plasma temperature distribution is described. The enthalpy probe technique was used to determine the plasma temperature. These results were correlated to the coating structure and the deposition efficiency.

2. Enthalpy Probe Theory

The enthalpy probe system included a water-cooled stainless steel probe, a closed loop probe-cooling water recirculation system, a gas sampling line, and a data acquisition and control unit. A three-axis positioning system was used for the movement of the probe. The enthalpy probe (Fig. 1) was a water-jacketed gas sampling and stagnation pressure probe with an outer diameter of 3.17 mm and an inner diameter of 0.66 mm.[1]

The probe-cooling system consisted of a variable speed positive displacement pump with a maximum delivery rating of 0.9 L/min. Deionized water, operating at a pressure of 6 MPa to avoid boiling, was used for the cooling supply. Table 1 shows the setting of the enthalpy probe system for the experiments.

The values of the local specific enthalpy of a plasma flow can be derived from an energy balance applied to the cooling water flow through a probe and with the gas sample continually being extracted from the plasma jet. A tare measurement is required for elimination of the external heat load to the probe. A valve in the gas line is closed to prevent gas from entering the probe, and observations of coolant temperature rise and flow rate are made. The valve is then opened, allowing a gas sample to flow through the probe. The same measurements are repeated, together with those of the steady gas sample temperature at the probe exit and steady gas sample flow rate.[2,3] The plasma enthalpy, h_i, is given by

$$h_i = h_o + \frac{c_{p,w}\left(\dot{m}_w,\, f\ \Delta T_f - \dot{m}_w, nf\ \Delta T_{nf}\right)}{\dot{m}_{gas}} \qquad \text{(Eq 1)}$$

and

$$h_o = c_{p,s} \cdot T_s \qquad \text{(Eq 2)}$$

where $c_{p,w}$ is the specific heat of the water, $m_{w,f}$ is the mass flow rate of the cooling water during sampling flow, and ΔT_f is the cooling water temperature difference during sample flow. The *nf* subscript stands for the nonflow conditions, when no sample is being drawn. The h_o represents the enthalpy of the gas sample at the probe outlet, determined by the temperature, T_s, and the specific heat, $c_{p,s}$, of the gas sample.

The velocity may be determined from Bernoullis's equation:

$$v = \sqrt{\frac{2(p_s - p_a)}{\rho(T)}} \qquad \text{(Eq 3)}$$

H.-D. Steffens and **T. Duda,** Institute of Materials Engineering, University of Dortmund, Otto-Hahn Str. 6, 44227 Dortmund, Germany.

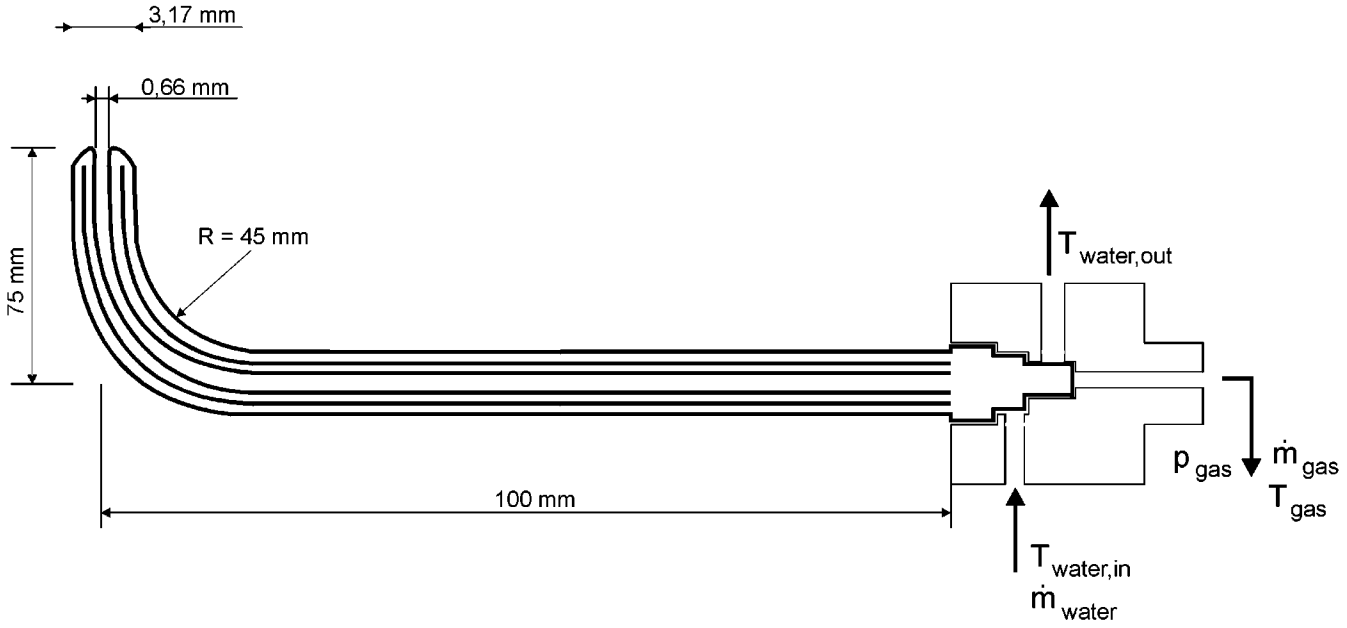

Fig. 1 Enthalpy probe

Table 1 Enthalpy probe system settings

Cooling flow rate	*mL/min*	450
Water pressure	*kPa*	6964
Sampling gas flow	*L/min*	5.4

where p_s is the stagnation pressure measured by the enthalpy probe when in nonflow mode, p is the static pressure, and $\rho(T)$ is the density of the plasma at the probe tip with respect to the plasma temperature.

Use of an enthalpy probe does not require the plasma to be in local thermodynamic equilibrium.[4] For determining the temperature, the transport, thermodynamic, and physical properties of the plasma gas as a function of the temperature have to be known. Figure 2 shows the calculation scheme for obtaining these properties. From the resulting tables, the plasma temperature can be determined by comparing the measured enthalpy values with the corresponding temperature data.

3. Enthalpy Probe Operation

For enthalpy probe measurements, steady-state conditions must be reached at each measurement location. In the experiments, it took between 7 and 10 s to reach a steady state, indicated by steadiness of the gas sample flow rate. Stagnation pressure, cooling water flow rate, and temperature rise were measured and stored during the tare measurement. The gas sampling valve was opened next, and the gas flow rate and gas temperature at the probe exit were measured together with the cooling water temperature rise and flow rate. The probe was then moved to another location, and the same procedure was repeated. Because in these experiments the radial distribution of the temperature at different axial locations was of interest, axial distances of 5 mm between the measurement locations were sufficient. With respect to the probe size, a radial distance of 2 mm was appropriate.

4. Experimental Setup

The torch used for the present study was a Sulzer Metco, Wohlen, Switzerland 9MB plasma gun commonly used for industrial spraying of coatings. The measurements were made using an argon/hydrogen mixture and two different anode designs. Table 2 lists the operational parameters. Figures 3 and 4 show the different geometries of the two anodes. Anode 1 was the standard Sulzer-Metco anode with an inner diameter (ID) of 5 mm, while anode 2 had a larger diameter (10 mm). For providing the same power input, current was increased to 590 A by spraying with the 10-mm ID nozzle. The thermal efficiencies were respectively 53% for the 5 mm nozzle and 44% for the 10 mm nozzle. They were calculated using following equation:

$$\eta = \frac{I \cdot U_{DC} - \dot{m}_w c_{p,w}(T_o - T_i)}{I \cdot U_{DC}} \quad \text{(Eq 4)}$$

where $T_o - T_i$ is the cooling water temperature rise during operation, $c_{p,w}$ is the specific heat of the water, $\dot{m}_{w,f}$ is the mass flow rate of the cooling water, I is the chosen arc current, and U_{DC} is the resulting arc voltage drop. Measurements were taken close to the nozzle exit to eliminate losses from cables.

Yttria-partially stabilized zirconia (7 wt.% Y_2O_3) was used in this investigation (Fig. 5). The fused and crushed particles with a nominal diameter of 10 to 60 μm were injected perpendicular to the plasma flow 3 mm downstream of the nozzle exit. The spraying distance was 80 mm.

The cast iron samples (10 by 15 by 60 mm), sand blasted before spraying, were placed on a substrate holder that allowed cooling from the backside with compressed air. A K-type thermocouple was adapted through a small hole from the backside near the substrate surface. This thermocouple was linked to a computer system, which controlled the pressured air flow in order to provide a constant substrate surface temperature of 150 °C. No

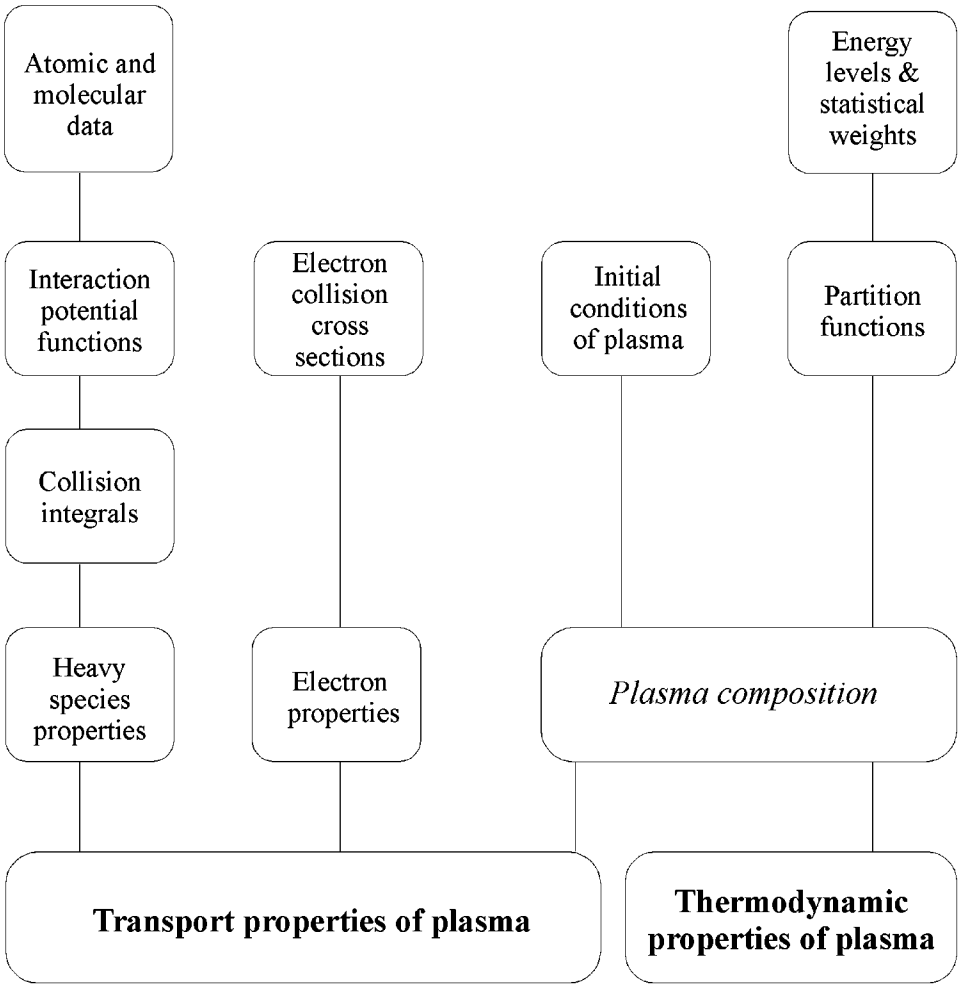

Fig. 2 Computing scheme [5]

Table 2 Experimental conditions

		Anode 1 5 mm ID		Anode 2 10 mm ID
Argon flow rate	*L/min*	. . .	40	. . .
Hydrogen flow rate	*L/min*	. . .	10	. . .
Current	*A*	500	. . .	590
Voltage	*V*	75	. . .	64
Carrier gas flow rate (Ar)	*L/min*	6	. . .	5
Substrate material	. . .	. . .	Cast iron	. . .
Powder feed rate	*g/min*	. . .	40	. . .
Substrate cooling medium	. . .	. . .	Pressured air	. . .

bond coat was used because the experiments were focused on the coating formation, with no special interest in bond strength or corrosion resistance. The deposition efficiency was measured by spraying on a mild steel cylinder (d = 110 mm, l = 80 mm) during a given time and by weighing the coated cylinder, knowing the previously calibrated powder feed rate. The cylinder was kept at 150 °C during spraying. The porosity of the coatings was determined by using an image analysis system, linked directly to the scanning electron microscope. Table 2 summarizes the experimental conditions.

5. Experimental Results and Discussion

5.1 Enthalpy Probe Measurements

The enthalpy probe measurements covered a range of axial distances from 40 to 100 mm. Figures 6 and 7 show typical radial profiles of the temperature at different axial positions for both nozzles.

No measurement could be performed using the enthalpy probe due to the level of heat load close to the nozzle. The heat load was further increased due to the release of significant amounts of energy from the recombination of hydrogen on the probe surface.[6] Therefore, measurements started 40 mm downstream of the nozzle exit to ensure a safe operation. At the location of the first measurement, the spreading of the jet was clearly visible. The maximum temperature of the standard nozzle was about 5100 K, and temperature distribution exhibited a strong gradient to the fringes of the jet (probably due to the higher pumping effect due to the higher velocity and higher level of turbu-

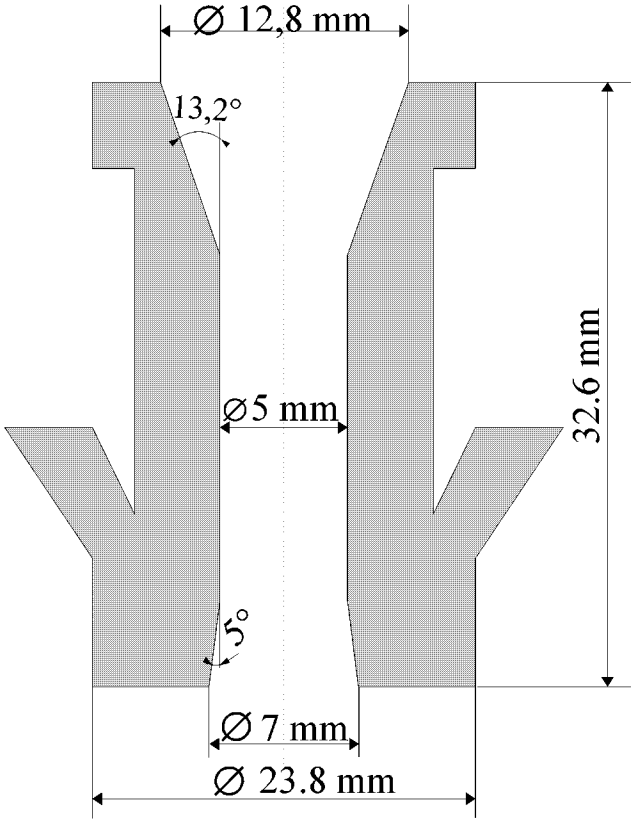

Fig. 3 Anode 1 with 5 mm ID

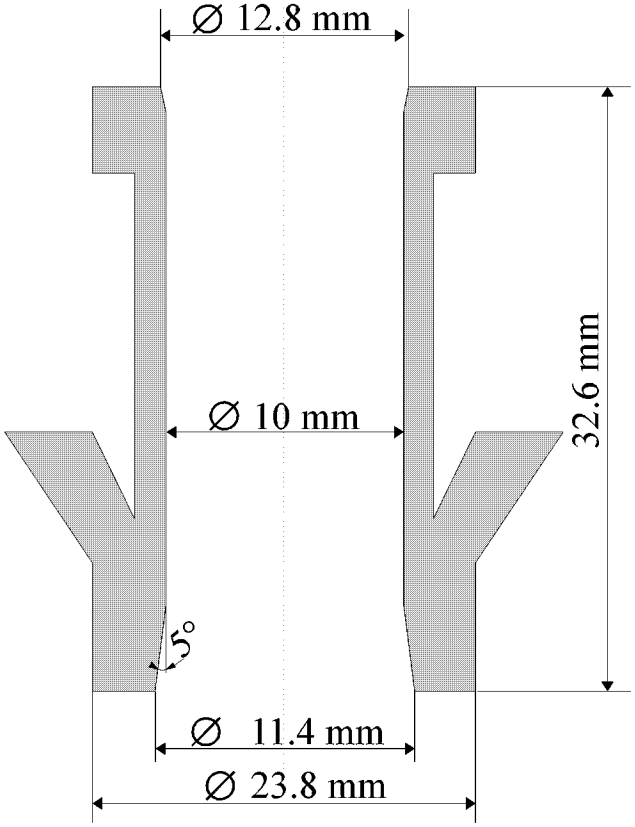

Fig. 4 Anode 2 with 10 mm ID

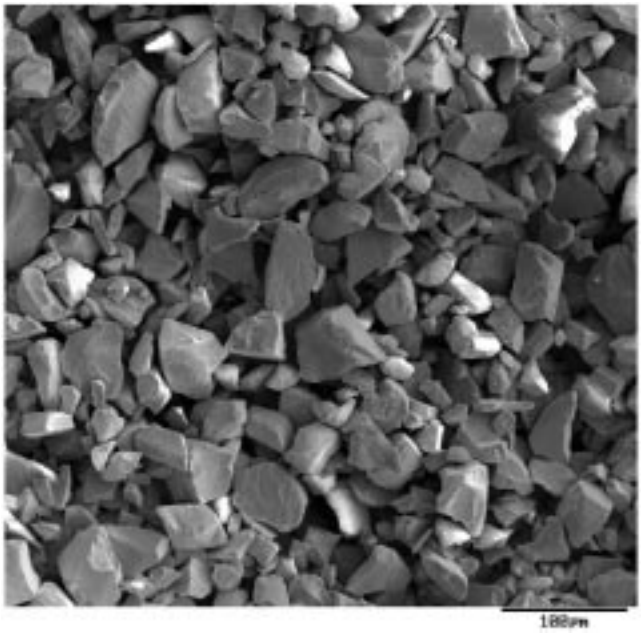

Fig. 5 Powder morphology, $ZrO_2 7Y_2O_3$, –60 + 10 µm

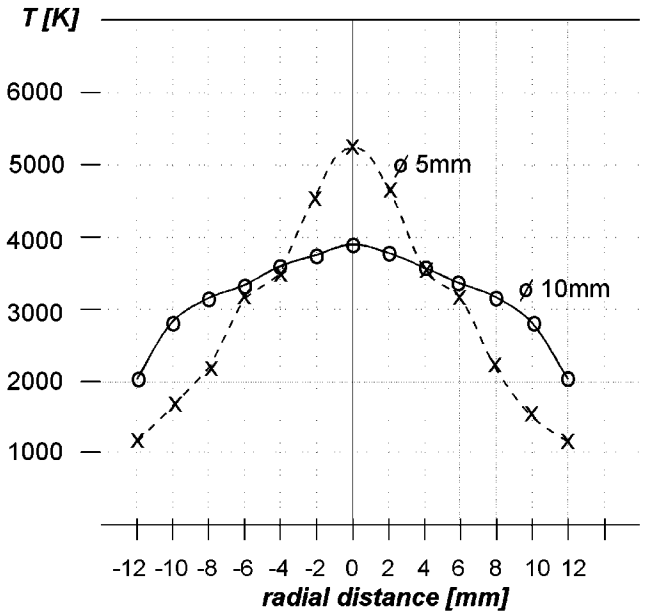

Fig. 6 Temperature distribution 40 mm downstream of the nozzle exit

lence).[7] The maximum temperature was roughly 1500 °C lower with the 10 mm nozzle, but the temperature distribution was more uniform, thus improving the heating of the particles traveling in the jet periphery. These different jet characteristics were emphasized by the temperature distribution 60 mm downstream of the nozzle exit. The maximum temperature at this measurement location was approximately the same, but the gradient to the fringes of the 5 mm anode was greater compared to that of the 10 mm anode.

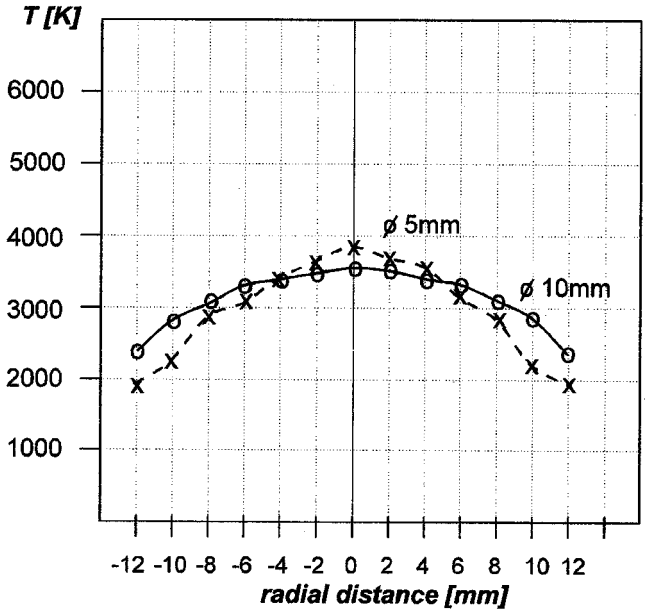

Fig. 7 Temperature distribution 60 mm downstream of the nozzle exit

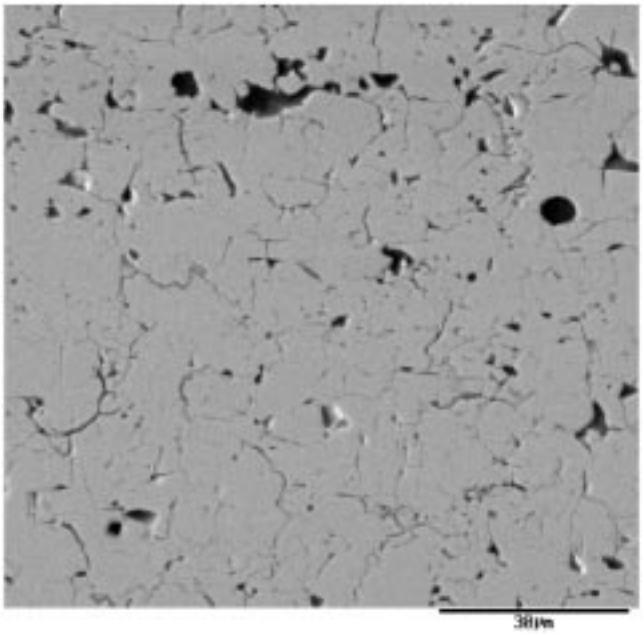

Fig. 8 Coating structure, obtained with anode 1, Ø 5 mm ID

5.2 Coating Structure

Figures 8 and 9 show typical scanning electron microscopy (SEM) pictures of cross sections of zirconia deposits for both nozzle designs. A decrease in density (4% for the 5 mm anode and 6% for the 10 mm) was observed for the deposits produced with the 10 mm ID nozzle compared to the 5 mm ID nozzle.

The fracture section of the zirconia deposit sprayed by the 10 mm ID nozzle, shown in Fig. 10, can be characterized by a columnar structure of individual splats, which were completely

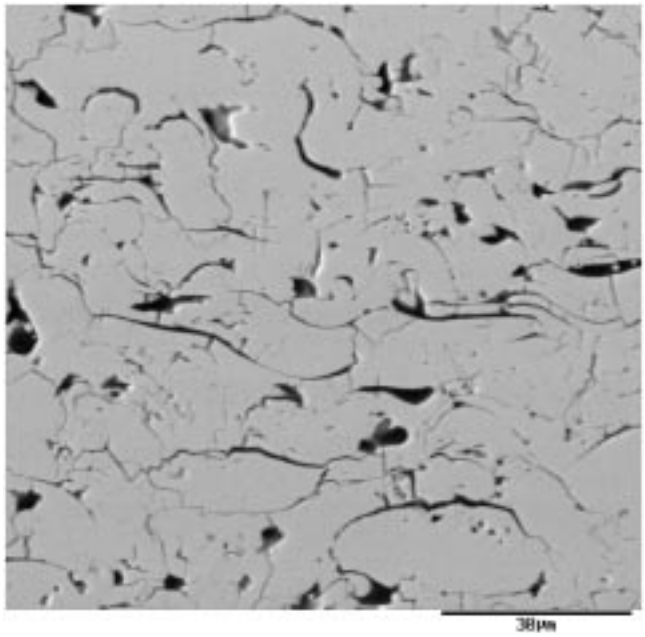

Fig. 9 Coating structure, obtained with anode 2, Ø 10 mm ID

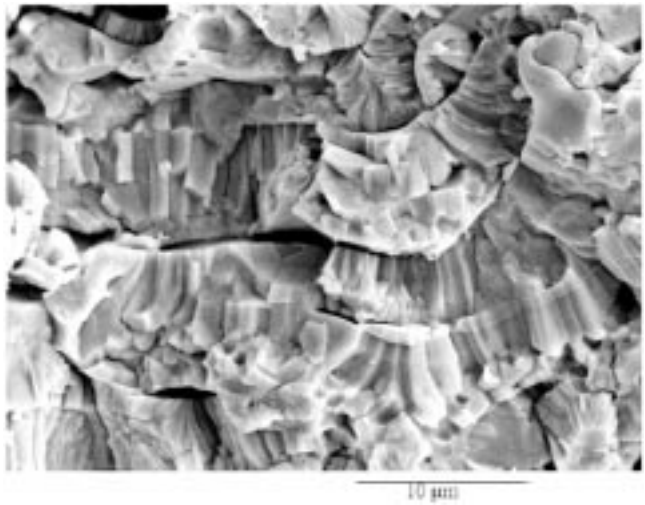

Fig. 10 SEM micrograph of the fracture section of anode 1, Ø 5 mm ID

melted. The fracture section of the coating produced by the 5 mm ID nozzle exhibited many partial particles, and a columnar structure was difficult to detect (Fig. 11).

5.3 Deposition Efficiency

The deposition efficiency improved from 40 to 58 % when spraying with the 10 mm diameter nozzle. This is due to the lower velocity of the plasma jet, which is a maximum of 250 m/s with the 10 mm ID anode compared to 500 m/s for the 5 mm ID anode at a location 40 mm downstream of the nozzle exit, calculated using Eq 3.[8] Additionally, the more uniform temperature distribution led to a decrease in the amount of nonmelted particles.

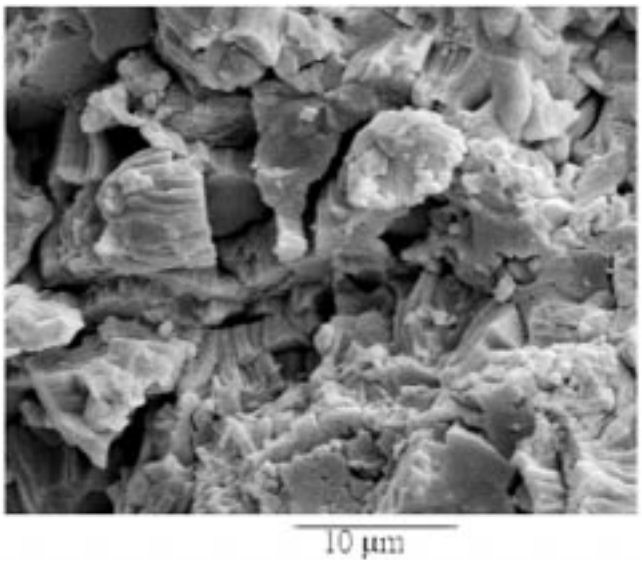

Fig. 11 SEM micrograph of the fracture section of anode 2, Ø 10 mm ID

6. Conclusions

Measurements of the plasma temperature for different nozzle designs in argon/hydrogen plasma jets were conducted using the enthalpy probe technique. The plasma jet temperatures were determined by comparing the measured enthalpy with the computed thermodynamic and transport properties. The influence of the anode geometry on enthalpy distribution and coating structure was examined. The preliminary results obtained are as follows.

- The enthalpy probe is a simple, reliable technique for determining the plasma enthalpy and temperature in relatively low temperature ($T < 9000$ K) regimes, where neither emission spectroscopy techniques nor thermocouple probing techniques could be used.
- The density of coating, sprayed with the standard anode geometry, exhibited a slightly more dense structure compared to the coating produced by the 10 mm ID anode. This can be explained by the higher velocity of the particles sprayed with the standard anode due to the higher gas velocities.
- The coating produced by the 10 mm ID nozzle exhibited a columnar structure, thus leading to the assumption that the high-temperature and thermal shock behavior were better compared to those of the coating sprayed using the standard nozzle. Additionally, the deposition efficiency was increased by 18% based on the more uniform temperature distribution and, therefore, a smaller amount of nonmolten particles.

Acknowledgments

The authors wish to thank Dr. Z. Babiak for technical assistance, Professor E. Pfender and Dr. J. Wilden for many fruitful discussions, and Dr. W.L.T. Chen for providing data on thermodynamic and transport properties.

References

1. *Operating and Service Manual*, Tekna Plasma Systems, Sherbrooke, PQ, Canada, 1993.
2. J. Grey, P.F. Jacobs, and M.P. Sherman: *Rev. Sci. Instrum.* 1962, vol. 33 (7), pp. 738–40.
3. A. Capetti and E. Pfender: *Plasma Chem. Plasma Proc.*, 1989, vol. 9 (2), pp. 329–41.
4. M. Rahmane, G. Soucy, M.I. Boulos, and R. Henne: in *Thermal Spray Industrial Applications*, C.C. Berndt and S. Sampath, eds. ASM INTERNATIONAL, Materials Park, OH 1994, pp. 355–59.
5. W.L.T. Chen: High Temperature Laboratory, University of Minnesota, Minneapolis, MN, private communication, 1993.
6. S.A. Jones: Master's Thesis, Thesis, University of Minnesota, Minneapolis, MN, 1994.
7. M.P. Planche, O. Betoule, J.F. Coudert, A. Grimaud, M. Vardelle, and P. Fauchais: in *Thermal Spray Coatings: Research, Design and Applications*, C.C. Berndt and T.F. Bernecki, eds., ASM INTERNATIONAL, Materials Park, OH 1993, pp. 81–87.
8. T. Duda: *Proc. 5th Workshop Plasmatechnik*, Technical University of Ilmenau, Ilmenau, Germany, 1996.